

1. DATA REPORT: SAND FRACTION, CARBONATE, AND ORGANIC CARBON CONTENTS OF LATE MIocene SEDIMENTS FROM SITE 1085, MIDDLE CAPE BASIN¹

Liselotte Diester-Haass,² Philip A. Meyers,³ Laurence Vidal,⁴ and
Gerold Wefer⁵

INTRODUCTION

Site 1085 is located on the continental rise of southwest Africa at a water depth of 1713 m off the mouth of the Orange River in the Cape Basin. The site is part of the suite of locations drilled during Leg 175 on the Africa margin to reconstruct the onset and evolution of the elevated biological productivity associated with the Benguela Current upwelling system (Wefer, Berger, Richter, et al., 1998). Three sediment samples were collected per section from Cores 170-1085A-28H through 45X (251–419 mbsf) to provide a survey of the sediment record of paleoproductivity from the middle late Miocene to the early Pliocene (~8.7–4.7 Ma), which is a period that includes the postulated northward migration and intensification of the Benguela Current and the establishment of modern circulation off southwest Africa (Siesser, 1980; Diester-Haass et al., 1992; Berger et al., 1998). Core 170-1085A-30H (270–279 mbsf) had essentially no recovery; this coring gap was filled with samples from Cores 170-1085B-29H and 30H (261–280 mbsf). The results of measurements of multiple paleoproductivity proxies are summarized in this report. Included in these proxies are the radiolarian, foraminiferal, and echinoderm components of the sand-sized sediment fraction. Opal skeletons of radiolarians (no diatoms were found) relate to paleoproductivity and water mass chemistry (Summerhayes et al., 1995; Lange and Berger, 1993; Nelson et al., 1995). The accumulation rates of benthic foraminifers are useful proxies for paleoproductivity (Herguera

¹Diester-Haass, L., Meyers, P.A., Vidal, L., and Wefer, G., 2001. Data report: Sand fraction, carbonate, and organic carbon contents of late Miocene sediments from Site 1085, Middle Cape Basin. In Wefer, G., Berger, W.H., and Richter, C. (Eds.), *Proc. ODP, Sci. Results*, 175, 1–23 [Online]. Available from World Wide Web: <http://www-odp.tamu.edu/publications/175_SR/VOLUME/CHAPTERS/SR175_01.PDF> [Cited YYYY-MM-DD]

²Zentrum für Umweltforschung, Universität des Saarlandes, D-66041 Saarbrücken, Federal Republic of Germany. A.L.Haass@t-online.de

³Department of Geological Sciences, University of Michigan, Ann Arbor MI 48109-1063 USA.

⁴Université Aix-Marseille, Europole de l'Arbois, BP 80, 13545 Aix en Provence Cedex, France.

⁵Fachbereich Geologie, Universität Bremen, D-28334 Bremen, Federal Republic of Germany.

and Berger, 1991; Nees, 1997; Schmiedl and Mackensen, 1997) because these fauna subsist on organic matter exported from the photic zone. Echinoderms also depend mainly on food supply from the photic zone (Gooday and Turley, 1990), and their accumulation rates are an additional paleoproductivity proxy. Concentrations of calcium carbonate (CaCO_3) and organic carbon in sediment samples are fundamental measures of paleoproductivity (e.g., Meyers, 1997). In addition, organic matter atomic carbon/nitrogen (C/N) ratios and $\delta^{13}\text{C}$ values can be used to infer the origin of the organic matter contained within the sediments and to explore some of the factors affecting its preservation and accumulation (Meyers, 1994).

METHODS

Sediment samples were divided for size-fraction microscopic and geochemical analyses. Subsamples were prepared for microscopic analyses by washing through 40- and 63- μm sieves. The <40- μm fraction residue was retained for later clay-mineral analyses, and the >40- μm fraction was used for coarse-fraction analysis and eventual isotope studies. In the coarse-fraction analysis, the >63- μm fraction was sieved into 63- to 125- μm , 125- to 250- μm , 250- to 500- μm , and >500- μm fractions. In each fraction, 800 grains (if present) were counted and up to 25 biogenic, lithogenic, and authigenic components were distinguished. The relative composition of the sand (>63 μm) and coarse silt (40- to 63- μm) fractions were calculated by multiplying the percentage of each individual component in each fraction by the weight of the fraction. These data are the basis for calculations of the mass accumulation rates (MAR) of components using the following formula:

$$\text{MAR}_{\text{comp}} = [(\% \text{ component} \times \text{MAR}_{\text{bulk sed}})/100] \times 1000 \text{ mg/cm}^2/\text{k.y.},$$

where MAR_{comp} and $\text{MAR}_{\text{bulk sed}}$ are the mass accumulation rates of various sediment components and the bulk sediment, respectively. The stratigraphy used for the calculation of linear sedimentation rates and MARs is based on oxygen isotope data of benthic foraminifers, a continuous X-ray fluorescence iron (XRF-Fe) profile, and orbital tuning.

Subsamples intended for geochemical analyses were first freeze-dried and then analyzed for CaCO_3 using the carbonate bomb technique of Müller and Gastner (1971). Weighed samples were reacted with 3-N HCl, and the volume of CO_2 released from each sample was measured and compared to the volumes released from known amounts of pure CaCO_3 to determine the percentage in the sample. The carbonate-free residue remaining after acid treatment was collected, rinsed, and dried for elemental CHN determinations. Organic carbon and nitrogen concentrations in the carbonate-free residues were directly measured with a Carlo Erba 1108 CHNS analyzer. This procedure involves heating the sample at 1020°C and measuring the combustion products by gas chromatography (Verardo et al., 1990). Known amounts of sulfanilamide ($\text{C}_6\text{H}_8\text{N}_2\text{O}_2\text{S}$) are used to calibrate the instrument and to calculate the quantities of carbon and nitrogen released from each sample. Total organic carbon (TOC) concentrations were calculated on a whole-sediment basis, adjusting for the carbonate concentrations determined from the bomb technique. C/N ratios were calculated on an atomic basis.

Organic $\delta^{13}\text{C}$ values were determined from analyses done in the stable isotope laboratory at the University of Michigan. Carbonate-free sediment samples were combusted at 800°C in sealed Vycor tubes in the presence of CuO and Cu. The $^{13}\text{C}/^{12}\text{C}$ ratios of organic carbon were determined with a Finnigan Delta-S mass spectrometer calibrated with the NBS-21 (graphite) standard. Data are corrected for ^{17}O and are expressed in conventional $\delta^{13}\text{C}$ notation relative to the PeeDee belemnite standard.

RESULTS

Changes in both sedimentation rate and composition occur over the 4-m.y. time span that we surveyed. The measured values of these various parameters are presented in Tables T1 and T2 and are summarized in individual depth plots. The linear sedimentation rate increases from 2 cm/k.y. below 370 mbsf to as great as 10.8 cm/k.y. above that depth (Fig. F1). The sand fraction comprises <2% of the total sediment below 370 mbsf; above this, its contribution increases sharply to as much as 6%, with strong cyclic variations (Fig. F2). The percentage of silt changes in similar patterns (Fig. F2).

The main components of the sand fraction are benthic and planktonic foraminifers (Fig. F3), but it also includes well-formed pyrite crystals (Fig. F4). The contribution of planktonic foraminifers increases from 40% at 420 mbsf to as high as 90% at 380 mbsf, and the contribution of benthic foraminifers decreases proportionally (Fig. F5). The amount of pyrite crystals changes in a fashion parallel to the benthic foraminifers—a continuous drop from 40% at 420 mbsf to about 10% at 370 mbsf (Fig. F4).

Accumulation rates of benthic and planktonic foraminifers (Fig. F6), whose cyclic variations are generally parallel, increase by a factor of 2–3 at 370 mbsf. Some exceptions, in which benthic foraminifers increase and planktonic foraminifers drop, occur in periods with strong fragmentation of planktonic foraminifers and point to loss of these sediment components by dissolution. In contrast, the accumulation rates of benthic foraminifers are low between 255 and 260 mbsf, whereas the planktonic foraminifer accumulation rates are rather high. These maxima occur during periods with weak carbonate dissolution, as indicated by fragmentation, and indicate good preservation of planktonic foraminifers.

Benthic foraminifer (>125 μm) accumulation rates in number per cm^2 per k.y. (Fig. F6) increase from <1000–3000 below 365 mbsf to >6000 at the maxima of the cycles in the uppermost Miocene. We calculated the numbers of benthic foraminifers both per gram of sediment and in number per cm^2 per k.y. in each fraction (Table T1). The values in all three fractions vary in parallel and show the same trend as the number per cm^2 per k.y. in total >125- μm fractions.

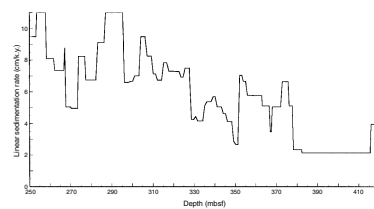
Opal skeletons of radiolarians have only been found in the interval between 285 and 325 mbsf (Fig. F7). The first maximum is simultaneous to a maximum in the accumulation rate of benthic foraminifers. Echinoids and ostracods (Fig. F8) increase above 290 mbsf. Accumulation rates of fish debris (Fig. F9) show the same trend as benthic foraminifers.

Cyclic changes of the two carbonate dissolution proxies (benthic/planktonic foraminifer ratios and fragmentation of planktonic foraminifers) (Fig. F10) vary generally in parallel, except for two intervals

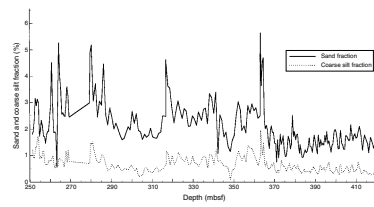
T1. Results of coarse fraction analysis, Site 1085, p. 21.

T2. Results of geochemical analysis, Site 1085, p. 22.

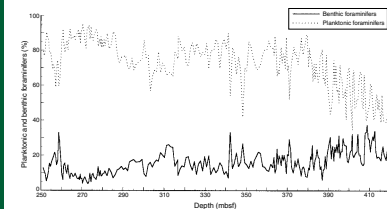
F1. Linear sedimentation rates, p. 7.



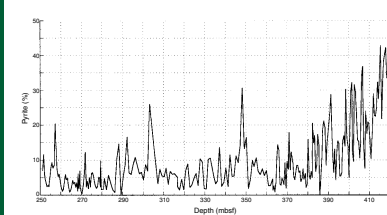
F2. Concentrations of the sand and coarse silt fractions of total sediment, p. 8.



F3. Concentrations of benthic and planktonic foraminifers in the sand fraction, p. 9.



F4. Concentration of pyrite crystals in the sand fraction, p. 10.



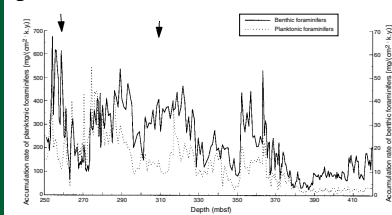
marked on Figure F10. From 420 to 380 mbsf, the benthic/planktonic foraminifer ratios decrease from 20%–40% to 5%–30% in the younger period. Maxima in fragmentation and mean values are higher in the 420–360 mbsf section than in the overlying unit.

The CaCO_3 concentration varies between 50 and 85 wt% (Fig. F11). The mass accumulation rate of CaCO_3 increases in three steps with time in the same way as the accumulation rate of benthic foraminifers (Fig. F12). Organic carbon percentages increase from <1 wt% below 360 mbsf to as great as 1.8 wt% in the younger section (Fig. F11). The mass accumulation rate of organic carbon increases parallel to that of CaCO_3 (Fig. F12). The C/N values vary from 19 to 7 (Table T2). Most of these atomic ratios are intermediate between unaltered algal organic matter (5–8) and fresh land plant material (25–35) (e.g., Emerson and Hedges, 1988; Meyers, 1994). Because of their setting offshore from a coastal desert, it is likely that the Site 1085 sediments contain mostly marine-derived organic matter in which the C/N values have been diagenetically elevated as a consequence of enhanced preservation (e.g., Meyers, 1997). Organic $\delta^{13}\text{C}$ values are mostly between $-20\text{\textperthousand}$ and $-23\text{\textperthousand}$, although values for some samples are as low as $-24\text{\textperthousand}$ (Table T3). These values are typical of marine organic matter (e.g., Meyers, 1994, 1997) and support the predominance of marine organic matter indicated by the C/N values of these samples (Table T3). Terrigenous particles have been counted in the 40- to 63- μm and >63- μm fractions (Fig. F13). The percentage in the >63- μm fraction is low (<0.5%) and percentages are up to 5% in the 40- to 63- μm fraction. Percentages decrease from 420 to 370 mbsf, but they increase again above 320 mbsf, with a maximum at 260 mbsf. The concentration of glauconite, which is believed to originate from lateral downslope transport from the shelf, has a temporal distribution like that of terrigenous particles (Fig. F14). The highest values of this mineral are found at 260 mbsf and are coincident with maxima in terrigenous matter.

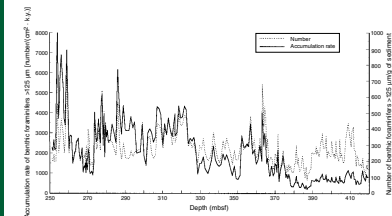
ACKNOWLEDGMENTS

Cheryl Stimpson, Rebecca Robinson, and Michela Arnaboldi performed the calcium carbonate and CHNS analyses. Various portions of this study were supported by grants from the Deutsche Forschungsgemeinschaft (LD-H, LV) and the United States Science Support Program (PAM).

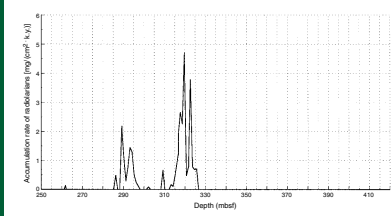
F5. Accumulation rates of benthic and planktonic foraminifers, p. 11.



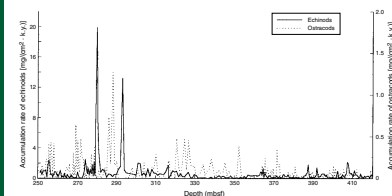
F6. Numbers of total benthic foraminifers and benthic foraminiferal accumulation rates, p. 12.



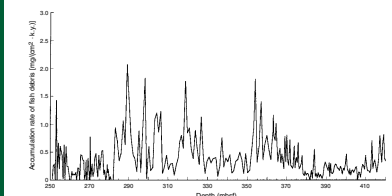
F7. Accumulation rates of radiolarians, p. 13.



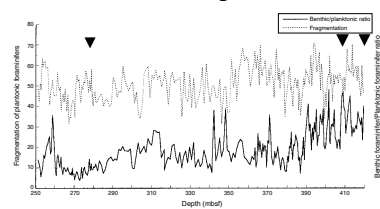
F8. Accumulation rates of echinoids and ostracods, p. 14.



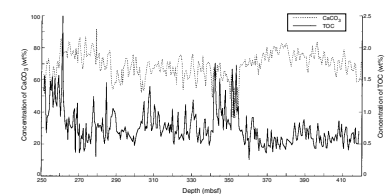
F9. Accumulation rates of fish debris, p. 15.



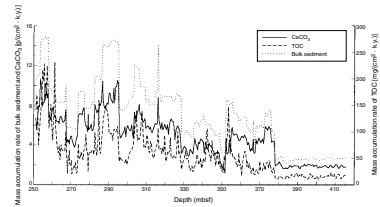
F10. Carbonate dissolution and percent fragmentation of planktonic foraminifers, p. 16.



F11. Concentrations of CaCO_3 and organic carbon, p. 17.

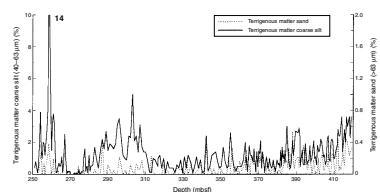


F12. Mass accumulation rates of bulk sediment, CaCO_3 , and organic carbon, p. 18.

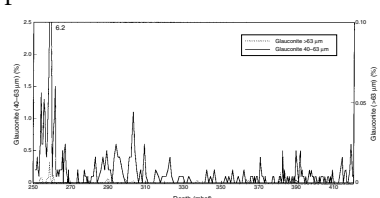


T3. Results of organic carbon isotope analysis, Site 1085, p. 23.

F13. Concentrations of terrigenous matter, p. 19.



F14. Concentrations of glauconite, p. 20.



REFERENCES

- Berger, W.H., Wefer, G., Richter, C., Lange, C.B., Giraudeau, J., Hermelin, O., and Shipboard Scientific Party, 1998. The Angola-Benguela upwelling system: paleoceanographic synthesis of shipboard results from Leg 175. In Wefer, G., Berger, W.H., and Richter, C., et al., *Proc. ODP, Init. Repts.*, 175: College Station, TX (Ocean Drilling Program), 505–531.
- Diester-Haass, L., Meyers, P.A., and Rothe, P., 1992. The Benguela Current and associated upwelling on the southwest African margin: a synthesis of the Neogene–Quaternary sedimentary record at DSDP Sites 362 and 352. In Summerhayes, C.P., Prell, W.L., and Emeis, K.C. (Eds.), *Upwelling Systems: Evolution Since the Early Miocene*. Geol. Soc. Spec. Publ. London, 64:331–342.
- Emerson, S., and Hedges, J.I., 1988. Processes controlling the organic carbon content of open ocean sediments. *Paleoceanography*, 3:621–634.
- Gooday, A.J., and Turley, C.M., 1990. Responses by benthic organisms to input of organic material to the ocean floor: a review. *Philos. Trans. R. Soc. London A*, 331:119–138.
- Herguera, J.C., and Berger, W.H., 1991. Paleoproductivity: glacial to postglacial change in the western equatorial Pacific, from benthic foraminifera. *Geology*, 19:1173–1176.
- Lange, C.B., and Berger, W.H., 1993. Diatom productivity and preservation in the western equatorial Pacific: the Quaternary record. In Berger, W.H., Kroenke, L.W., Mayer, L.A., et al., *Proc. ODP, Sci. Results*, 130: College Station, TX (Ocean Drilling Program), 509–523.
- Meyers, P.A., 1994. Preservation of elemental and isotopic source identification of sedimentary organic matter. *Chem. Geol.*, 144:289–302.
- _____, 1997. Organic geochemical proxies of paleoceanographic, paleolimnologic, and paleoclimatic processes. *Org. Geochem.*, 27:213–250.
- Müller, G., and Gastner, M., 1971. The “Karbonat-Bombe,” a simple device for the determination of the carbonate content in sediments, soils and other materials. *Neues. Jahrb. Mineral. Monatsh.*, 10:466–469.
- Nees, S., 1997. Late Quaternary palaeoceanography of the Tasman Sea: the benthic foraminiferal view. *Palaeogeogr., Palaeoclimatol., Palaeoecol.*, 131:365–389.
- Nelson, D.M., Treguer, P., Brzezinski, M.A., Leynaert, A., and Queguiner, B., 1995. Production and dissolution of biogenic silica in the ocean: revised global estimates, comparison with regional data and relationship to biogenic sedimentation. *Global Biogeochem. Cycles*, 9:359–372.
- Schmiedl, G., and Mackensen, A., 1997. Late Quaternary paleoproductivity and deep water circulation in the eastern South Atlantic Ocean: evidence from benthic foraminifera. *Palaeogeogr., Palaeoclimatol., Palaeoecol.*, 130:43–80.
- Siesser, W.G., 1980. Late Miocene origin of the Benguela upwelling system off northern Namibia. *Science*, 208:283–285.
- Summerhayes, C.P., Kroon, D., Rosell-Melé, A., Jordan, R.W., Schrader, H.-J., Hearn, R., Villanueva, J., Grimalt, J.O., and Eglinton, G., 1995. Variability in the Benguela Current upwelling system over the past 70,000 years. *Prog. Oceanogr.*, 35:207–251.
- Verardo, D.J., Froelich, P.N., and McIntyre, A., 1990. Determination of organic carbon and nitrogen in marine sediments using the Carlo Erba NA-1500 Analyzer. *Deep-Sea Res. Part A*, 37:157–165.
- Wefer, G., Berger, W.H., and Richter, C., et al., 1998. *Proc. ODP, Init. Repts.*, 175: College Station, TX (Ocean Drilling Program).

Figure F1. Linear sedimentation rates.

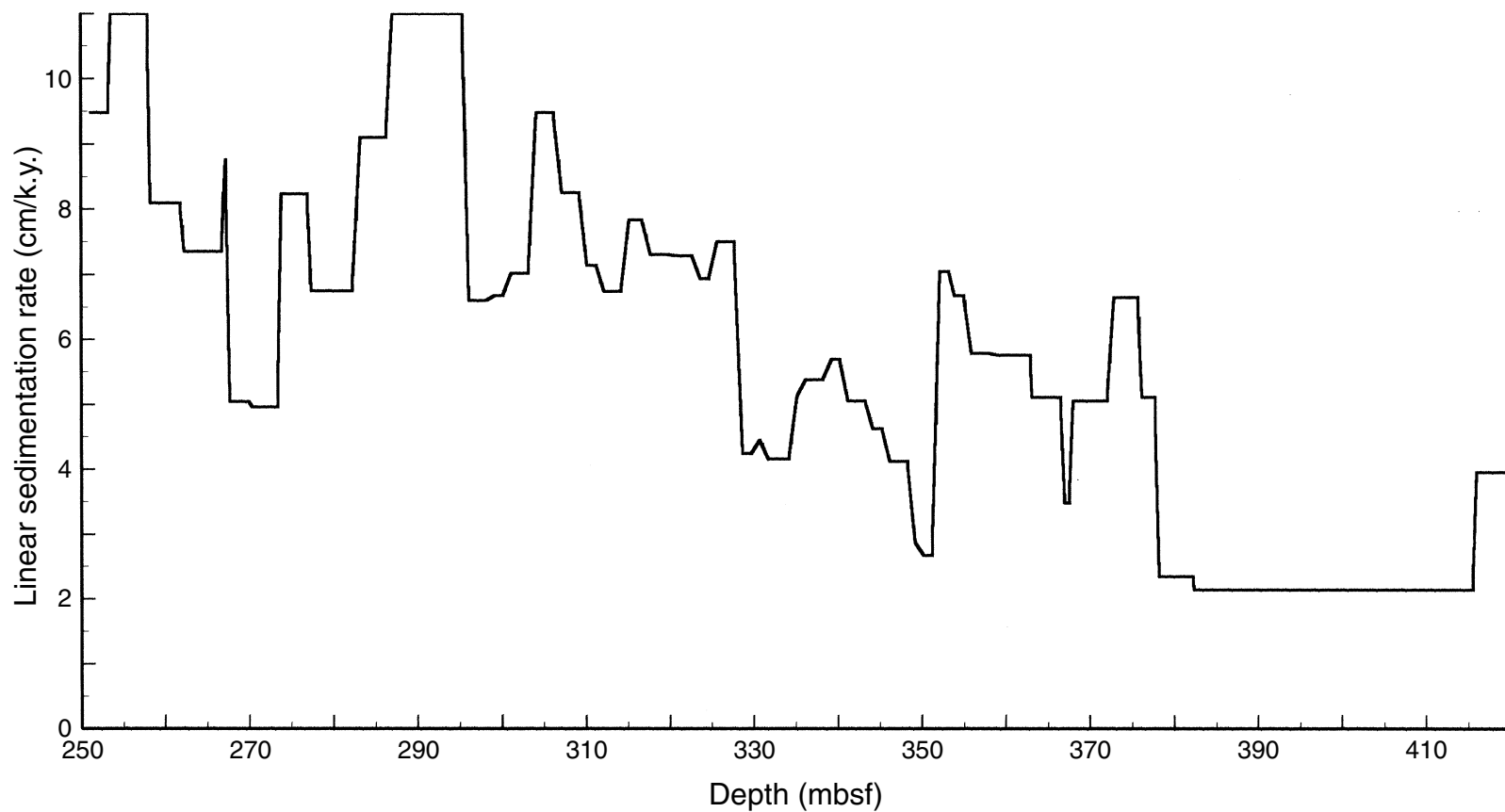


Figure F2. Concentrations of the sand ($>63 \mu\text{m}$) and coarse silt (40 to $63 \mu\text{m}$) fractions of total sediment.

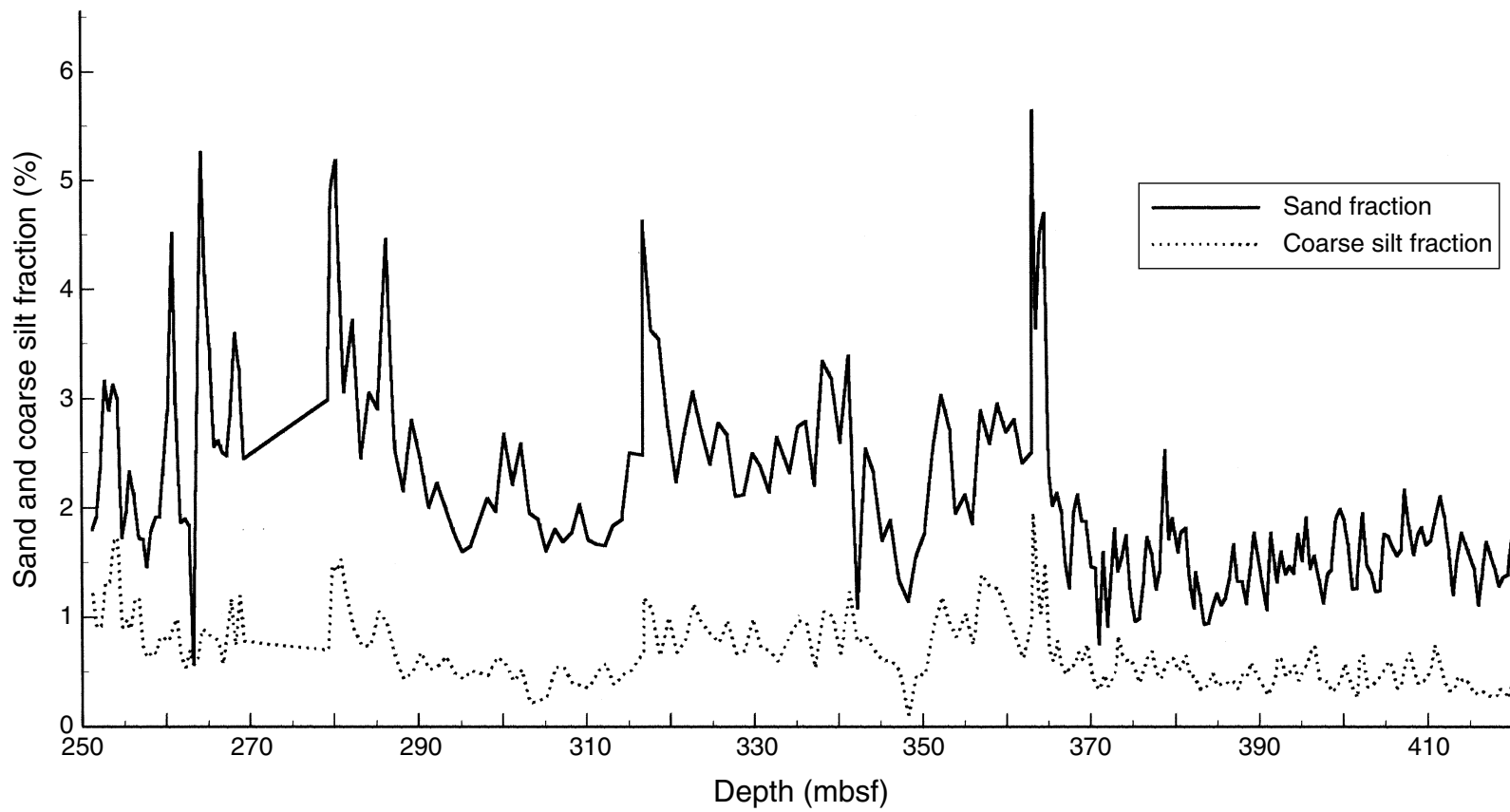


Figure F3. Concentrations of benthic and planktonic foraminifers in the sand fraction.

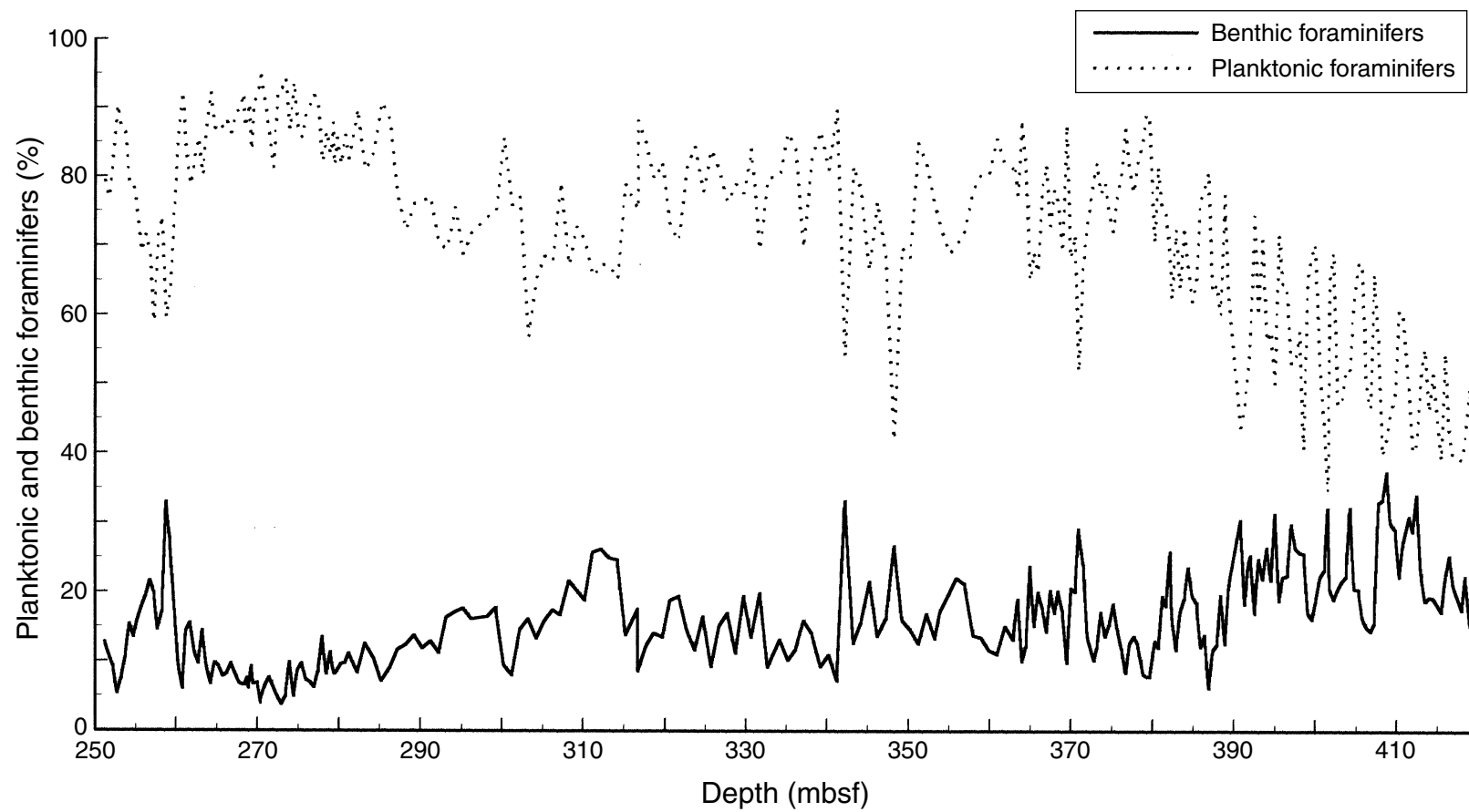


Figure F4. Concentration of pyrite crystals in the sand fraction.

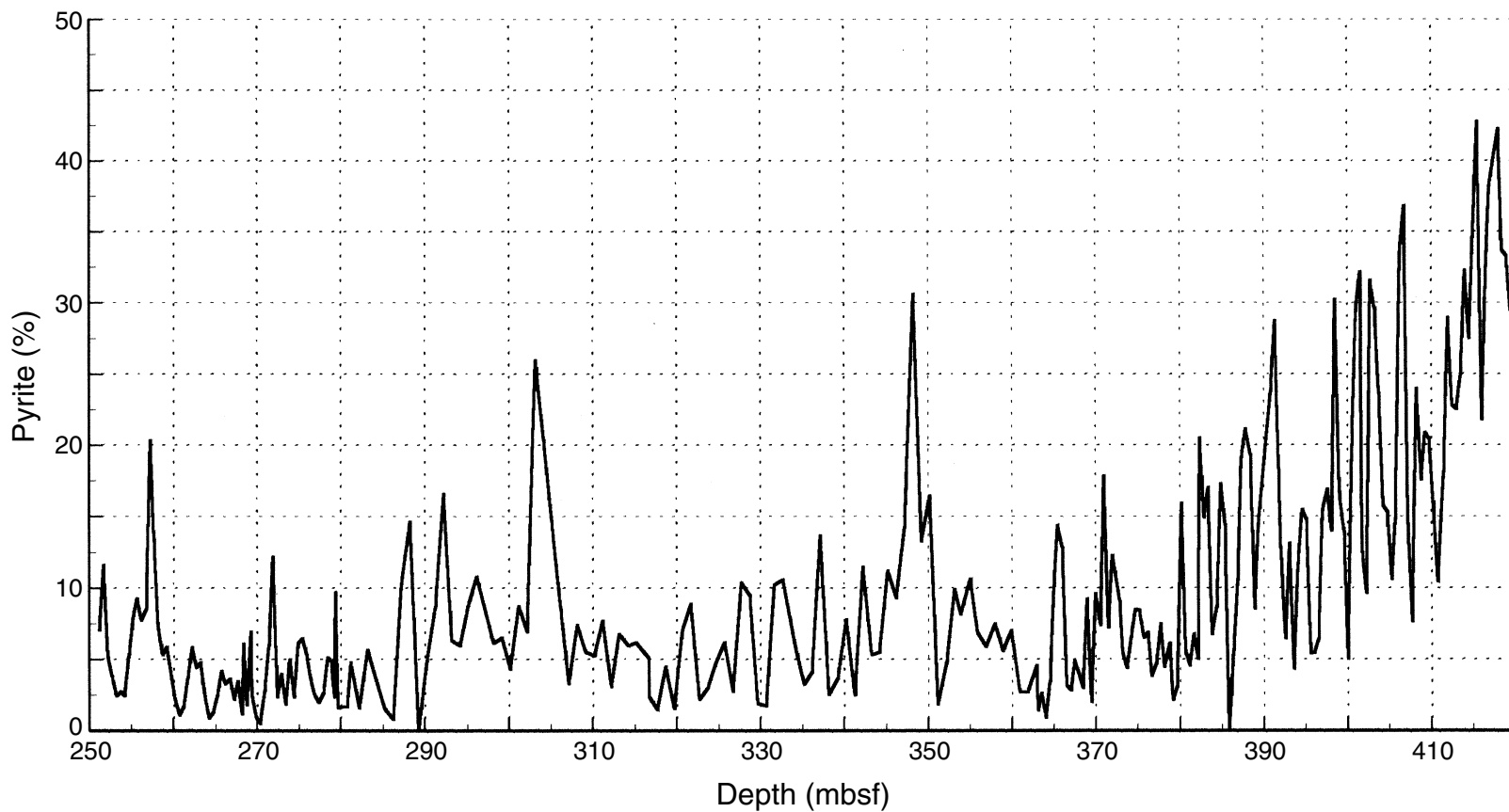


Figure F5. Accumulation rates of benthic and planktonic foraminifers in the sand fraction. Arrows mark intervals where both parameters do not covary.

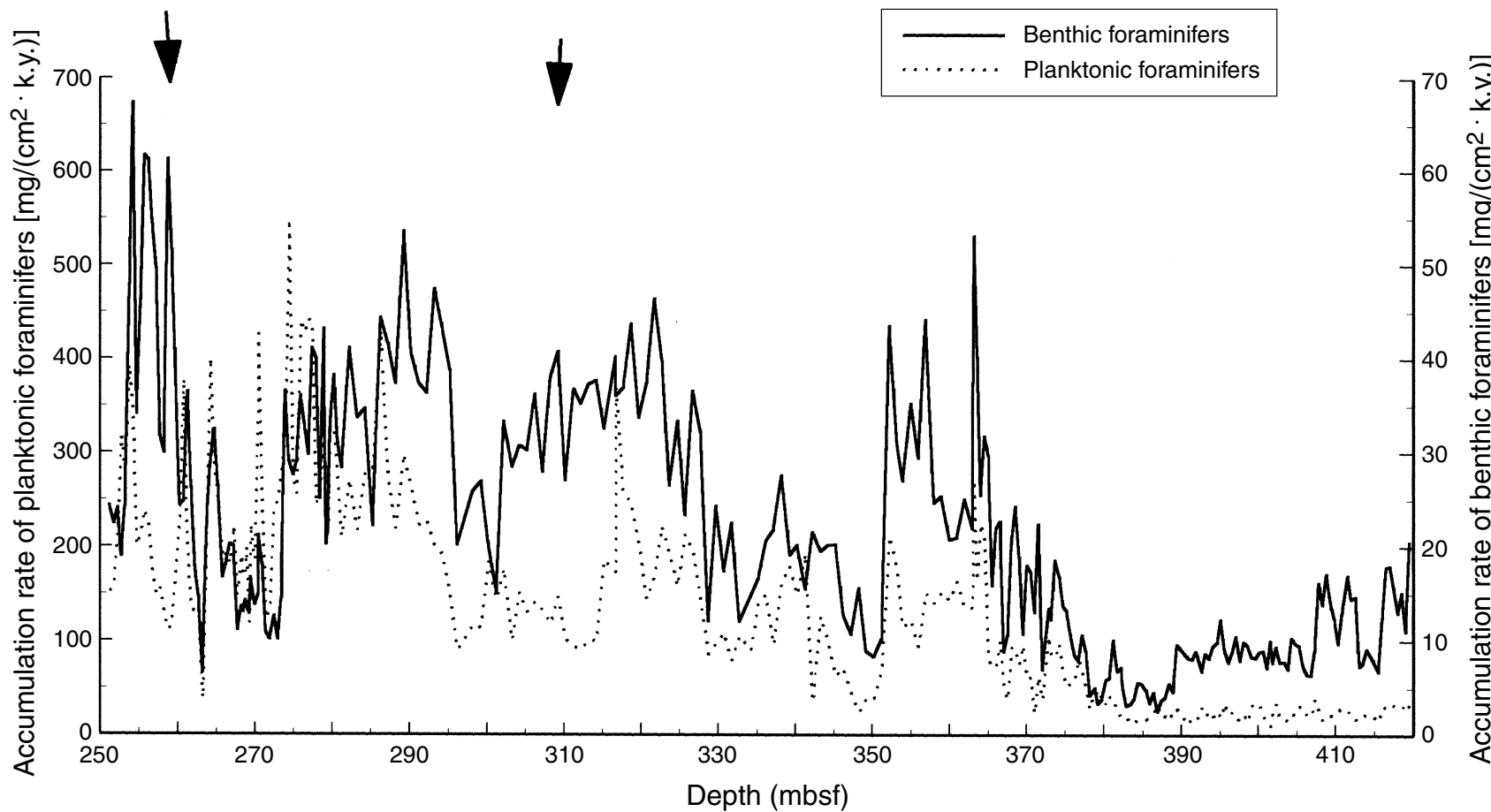


Figure F6. Numbers of total benthic foraminifers ($>125 \mu\text{m}$) per gram of sediment and benthic foraminiferal accumulation rates.

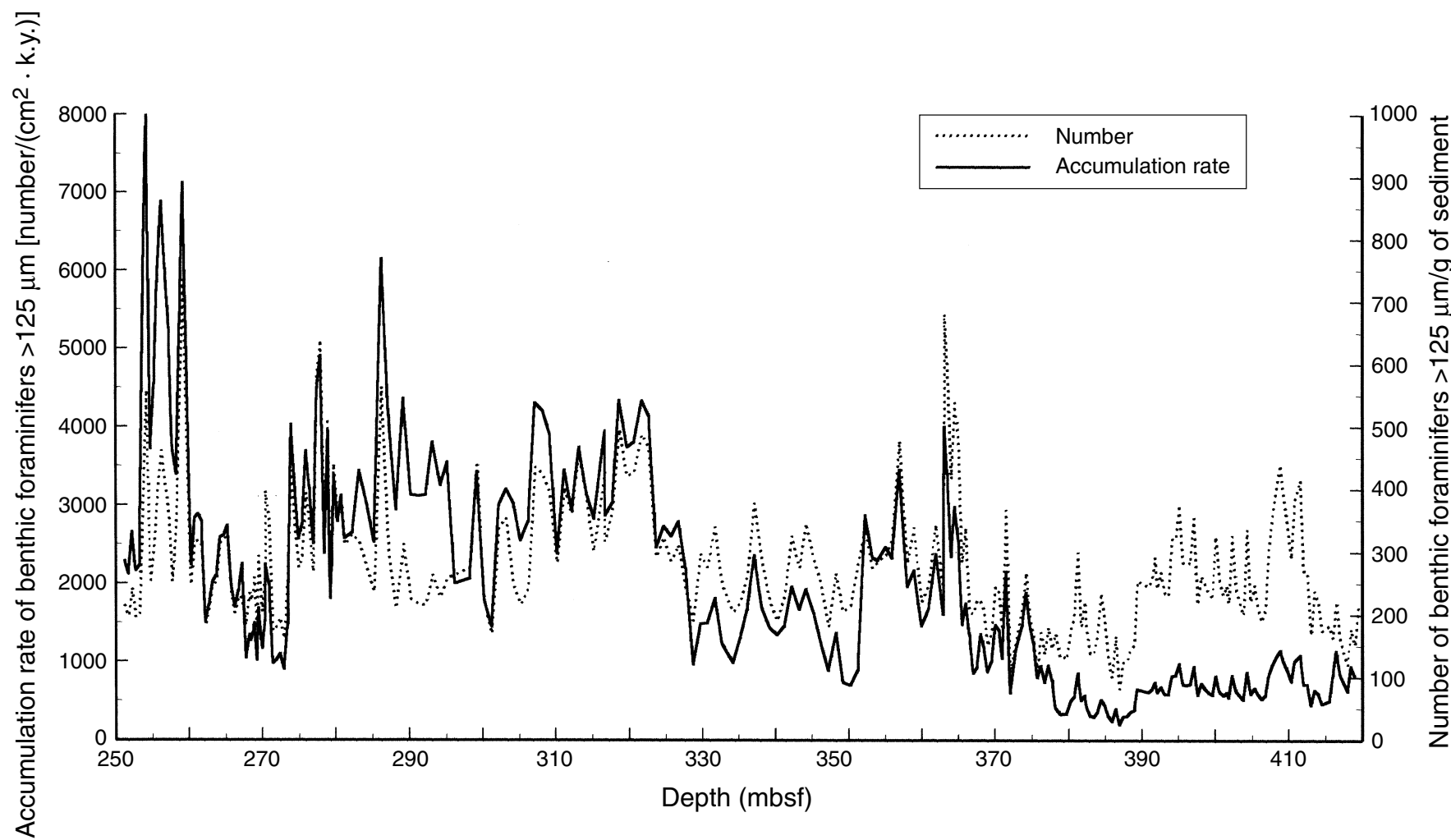


Figure F7. Accumulation rates of radiolarians.

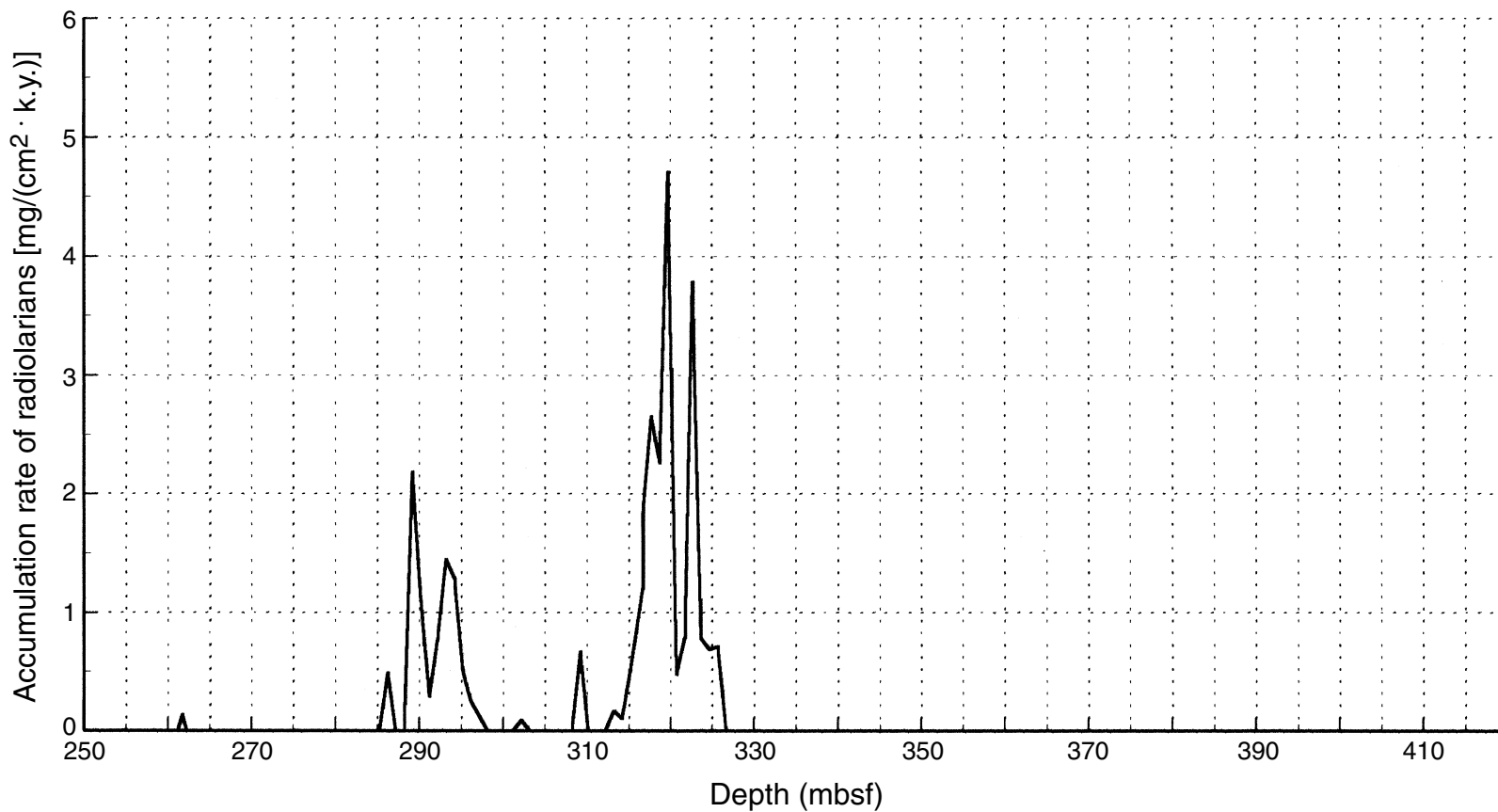


Figure F8. Accumulation rates of echinoids and ostracods.

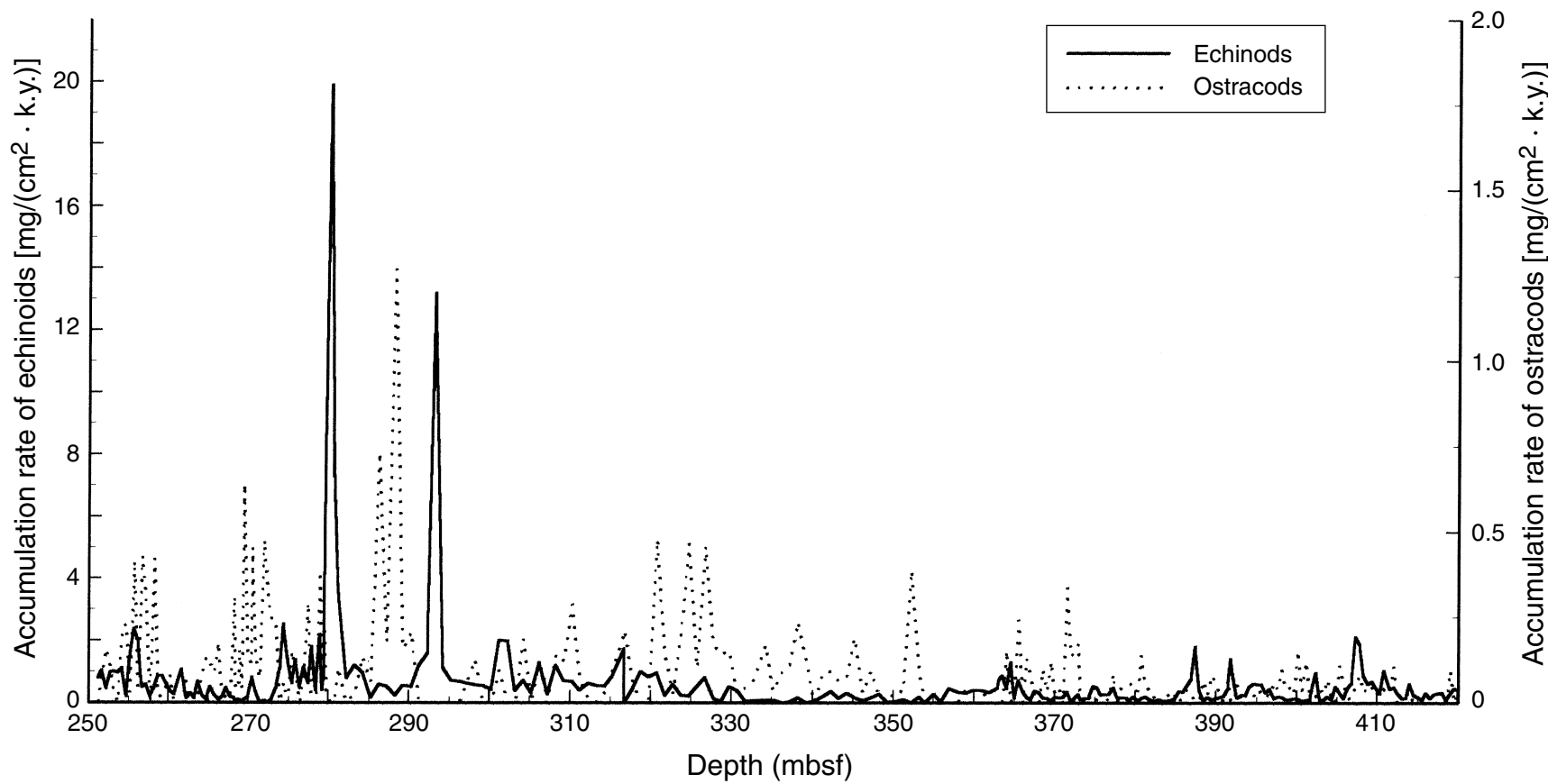


Figure F9. Accumulation rates of fish debris.

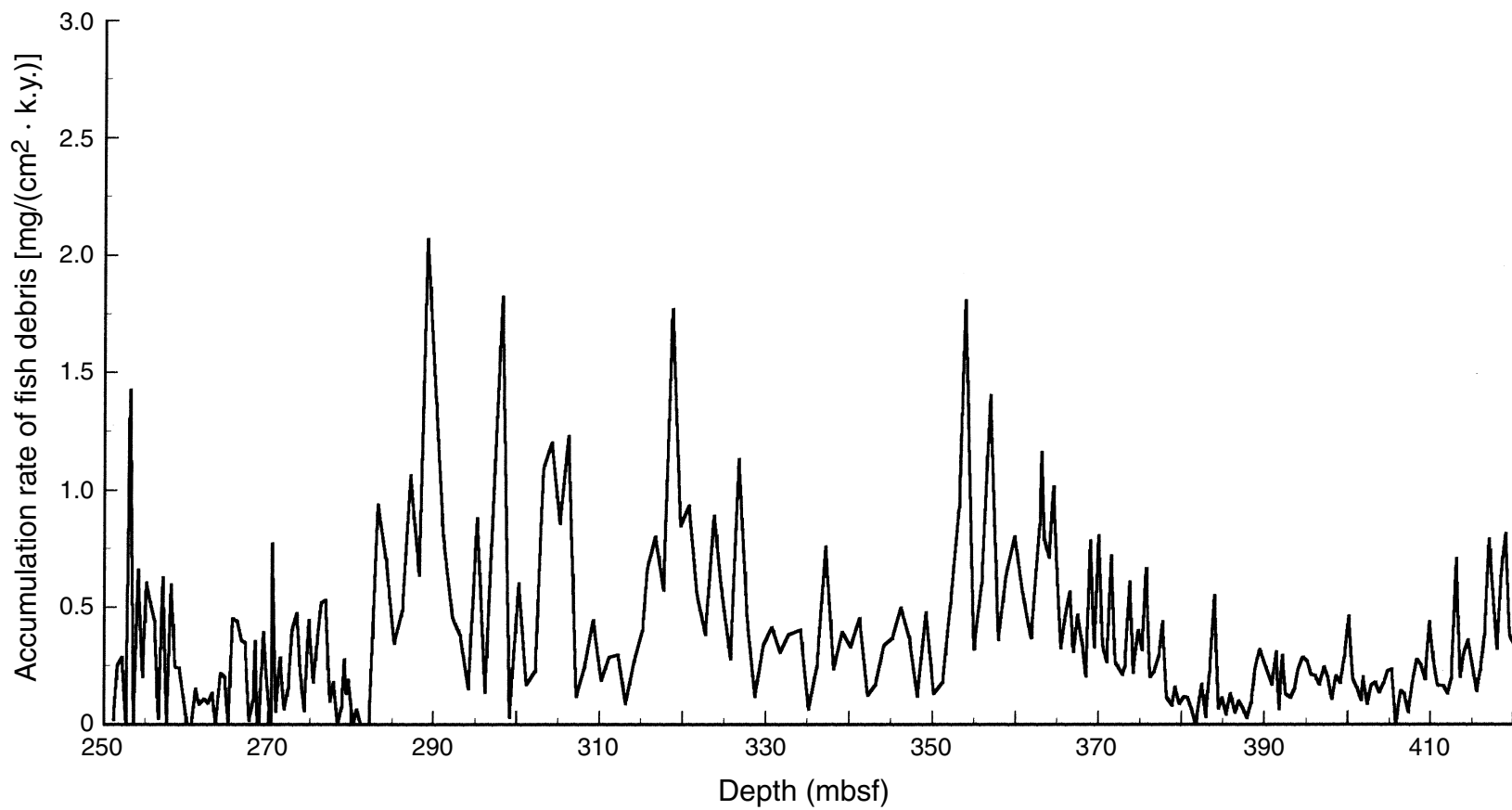


Figure F10. Carbonate dissolution as indicated by means of benthic/planktonic foraminiferal ratios [benthic/(benthic+planktonic) × 100] and percent fragmentation of planktonic foraminifers [fragments/(fragments+whole tests) × 100]. Arrows mark intervals where both parameters do not covary.

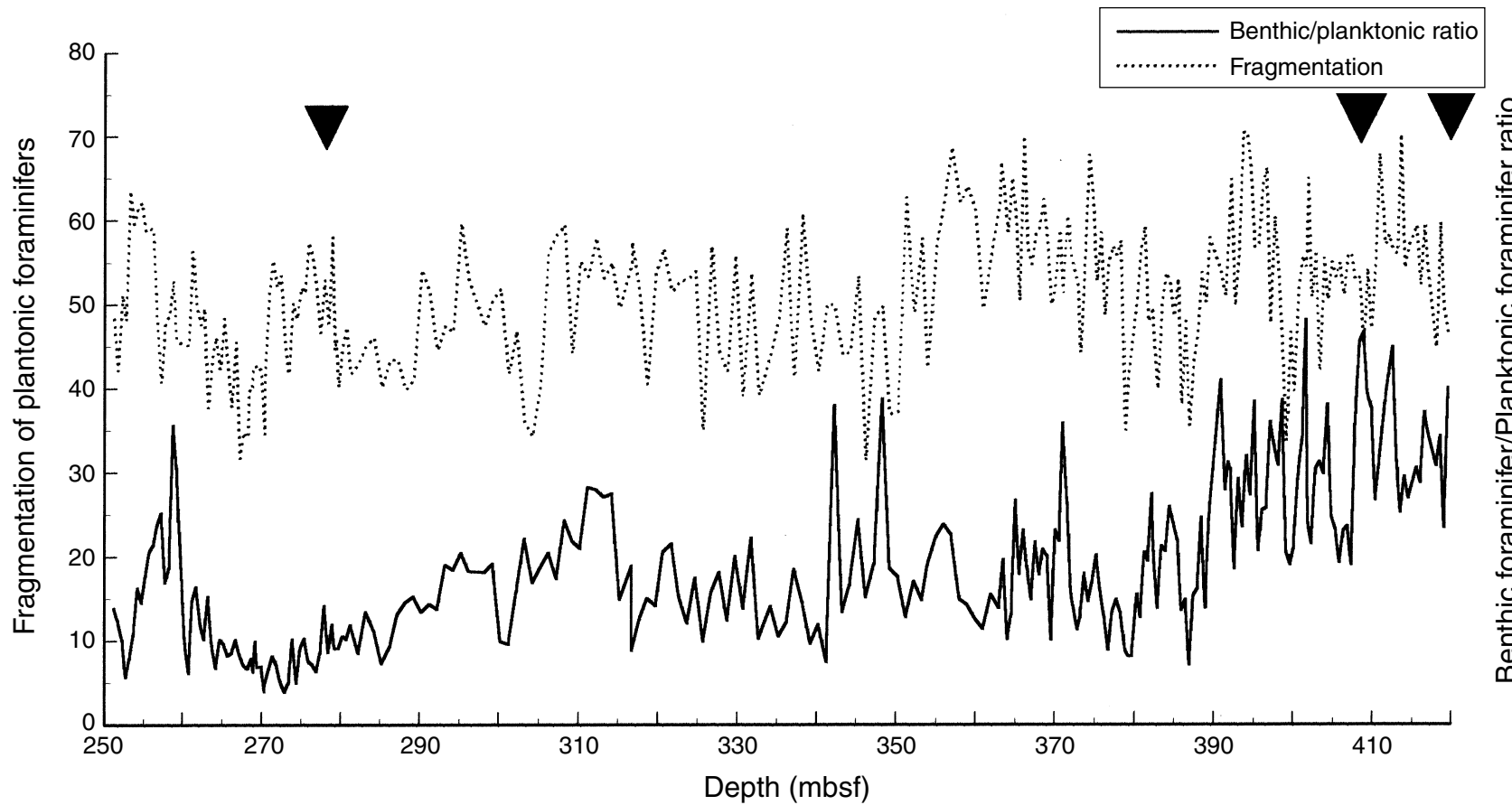


Figure F11. Concentrations of CaCO_3 and organic carbon.

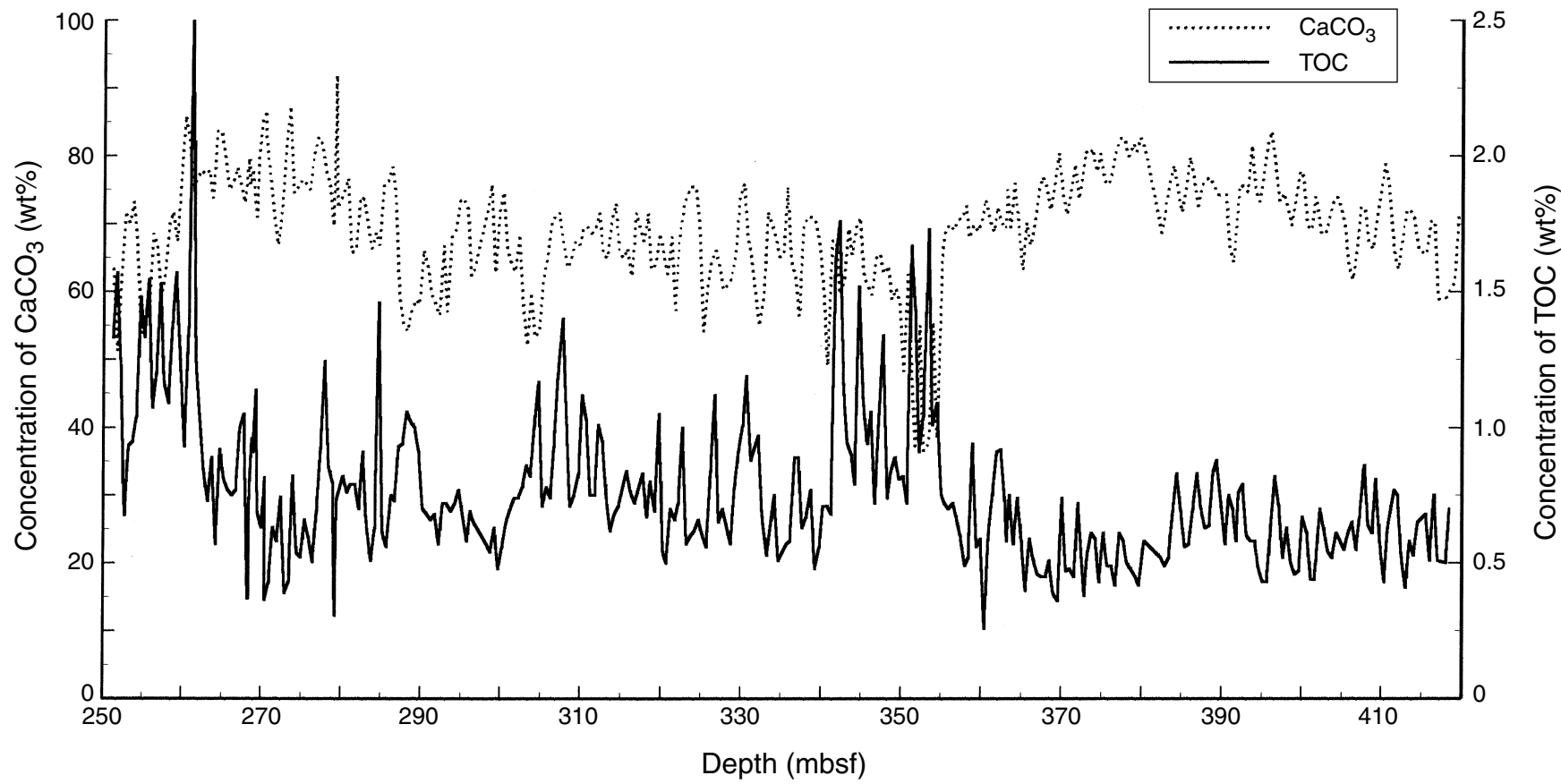


Figure F12. Mass accumulation rates of bulk sediment, CaCO_3 , and organic carbon.

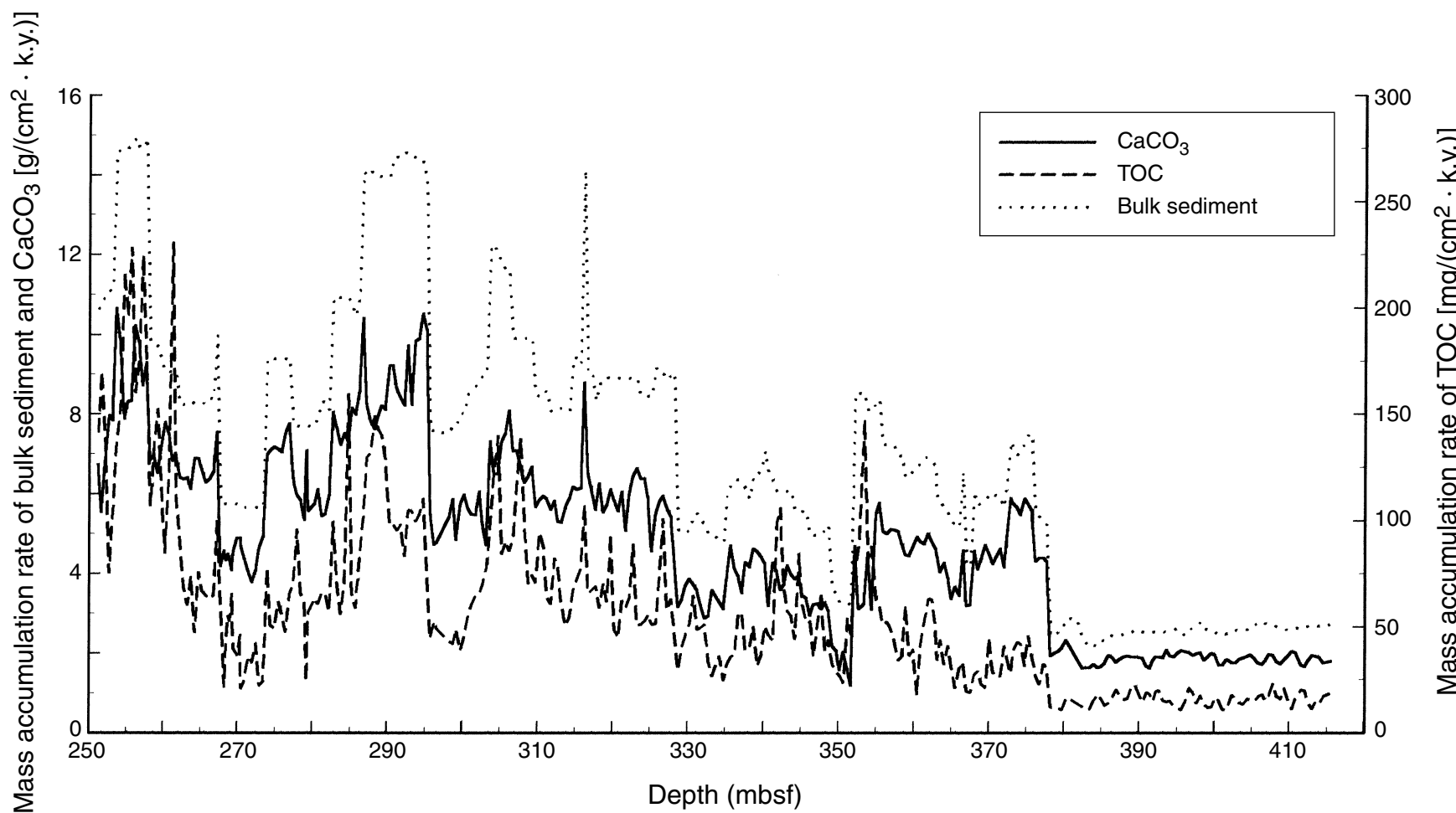


Figure F13. Concentrations of terrigenous matter in the sand and coarse silt fractions.

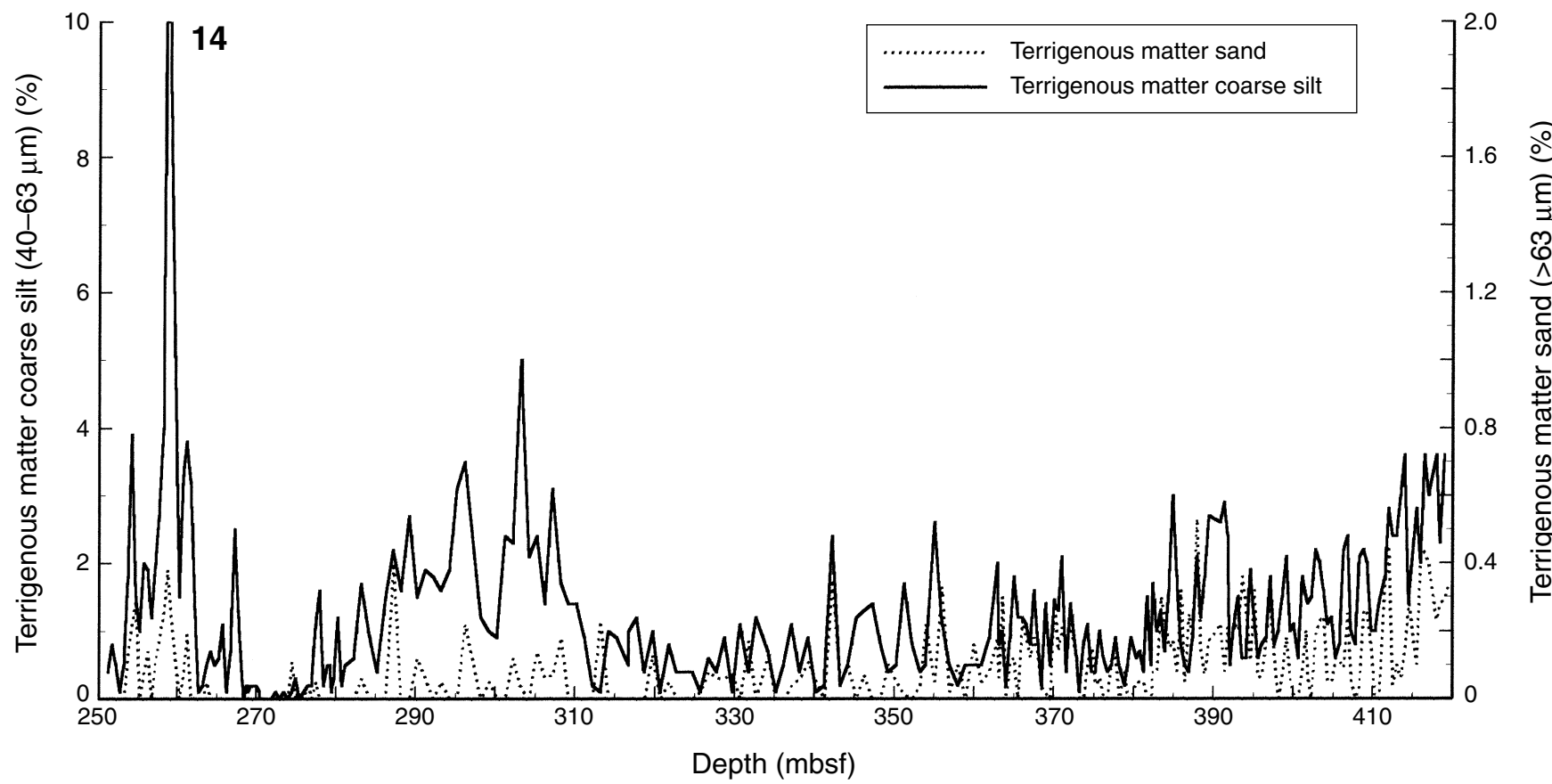


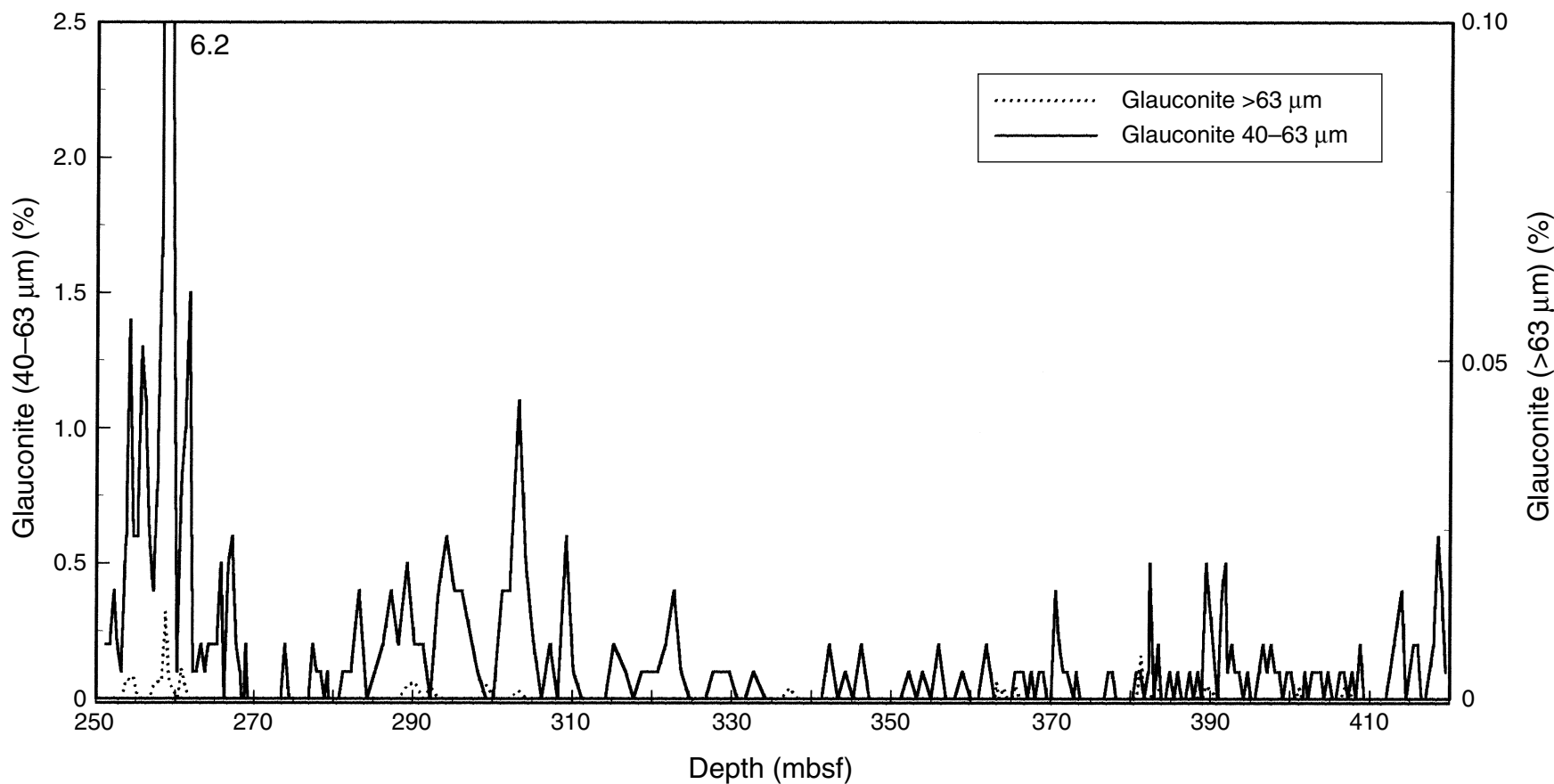
Figure F14. Concentrations of glauconite.

Table T1. Results of coarse fraction analysis, Site 1085.

Leg, hole, core, section, interval (cm)	Depth (mbsf)	Sand (%)	LSR (cm/k.y.)	Pyrite >63-µm fraction (%)	Benthic foraminifers (%)	AR benthic foraminifers (mg/[cm ² × k.y.])	Planktonic foraminifers (%)	AR planktonic foraminifers (mg/[cm ² × k.y.])	Number of benthic foraminifers per gram of sediment			Benthic foraminifer AR in fraction (number/[cm ² × k.y.])			AR (mg/[cm ² × k.y.])					
									>500	>250	>125	>500 µm	>250 µm	>125 µm	AR in 125- to 1000-µm fraction	AR in 125- to 1000-µm fraction	AR in 125- to 1000-µm fraction			
175-1085A-28H-1, 52	251.22	1.80	9.48	7.0	12.75	24.35	79.38	151.60	0.75	11.55	202.55	215	8	123	2151	2281	0	0.00	0.78	0.01
175-1085A-28H-1, 102	251.72	1.92	9.48	8.6	10.84	22.46	76.79	159.08	0.60	5.21	190.63	196	7	56	2060	2123	0	0.08	1.04	0.12
175-1085A-28H-2, 2	252.22	2.36	9.48	5.2	9.29	24.12	83.42	216.59	0.70	13.26	227.61	242	8	146	2503	2657	0	0.16	0.47	0.11
175-1085A-28H-2, 52	252.72	3.16	9.48	2.9	5.41	18.95	90.27	316.21	1.14	18.84	174.53	195	13	209	1936	2157	0	0.11	0.98	0.00
175-1085A-28H-2, 102	253.22	2.89	9.48	1.9	7.51	24.31	86.68	280.55	0.39	15.38	183.49	199	4	172	2053	2229	0	0.03	1.00	0.44
175-1085A-28H-3, 2	253.72	3.13	12.22	2.1	10.54	47.91	86.27	392.13	0.82	17.83	372.12	391	12	259	5411	5683	0	0.00	0.95	0.00
175-1085A-28H-3, 52	254.22	3.00	12.22	1.6	15.34	67.40	79.04	347.30	0.98	22.82	532.90	557	14	335	7814	8163	0	0.22	1.10	0.15
175-1085A-28H-3, 102	254.72	1.73	12.22	1.0	13.48	34.13	79.03	200.09	0.27	9.91	243.34	254	4	145	3568	3718	0	0.23	0.20	0.08
175-1085A-28H-4, 2	255.22	1.96	12.22	3.8	16.09	46.29	74.52	214.39	0.72	12.86	296.33	310	11	189	4345	4545	0	0.03	1.47	0.21
175-1085A-28H-4, 52	255.72	2.33	12.22	2.8	17.91	61.71	68.97	237.65	0.75	11.23	384.06	396	11	166	5679	5856	0	0.41	2.38	0.15

Leg, hole, core, section, interval (cm)	Depth (mbsf)	Benthic/planktonic foraminifer ratio	Fragmentation of planktonic foraminifers (%)	Carbonate dissolution		Terrigenous matter >63-µm fraction			Terrigenous matter 40- to 63-µm fraction			Other components of the >63-µm fraction			
				AR (mg/[cm ² × k.y.])	Quartz + rock debris (%)	AR quartz + rock debris (mg/[cm ² × k.y.])	Mica (%)	AR mica (mg/[cm ² × k.y.])	Quartz + mica (%)	AR quartz + mica (mg/[cm ² × k.y.])	Pyrite (%)	Glaconite (%)	Relict shells (%)	Mollusks (%)	
175-1085A-28H-1, 52	251.22	13.84	48.35	0.40	0.76	0.40	0.52	0.60	0.77	1.00	1.29	7.05	0	0	0
175-1085A-28H-1, 102	251.72	12.37	42.11	0.13	0.27	0.80	0.78	0.50	0.49	1.30	1.27	11.58	0	0	0
175-1085A-28H-2, 2	252.22	10.02	51.19	1.79	4.65	0.50	0.51	1.60	1.62	2.10	2.12	5.10	0	0	0
175-1085A-28H-2, 52	252.72	5.65	48.07	0.23	0.81	0.10	0.15	0.10	0.15	0.20	0.29	3.78	0	0	0
175-1085A-28H-2, 102	253.22	7.97	63.57	2.54	8.22	0.50	0.74	1.20	1.77	1.70	2.51	2.47	0	0	0
175-1085A-28H-3, 2	253.72	10.89	59.56	0.14	0.64	1.80	4.43	0.60	1.48	2.40	5.91	2.75	0.07	0	0
175-1085A-28H-3, 52	254.22	16.25	61.64	2.66	11.69	3.90	9.85	1.00	2.53	4.90	12.38	2.44	0.07	0	0
175-1085A-28H-3, 102	254.72	14.57	62.12	1.87	4.73	1.50	1.99	2.60	3.44	4.10	5.43	5.38	0.08	0	0
175-1085A-28H-4, 2	255.22	17.76	58.72	0.59	1.70	1.00	1.42	2.20	3.13	3.20	4.56	8.08	0	0	0
175-1085A-28H-4, 52	255.72	20.61	59.08	2.88	9.92	2.00	2.62	2.50	3.27	4.50	5.89	9.28	0	0	0

Note: LSR = linear sedimentation rate, AR = accumulation rate. Only a portion of this table appears here. The entire table is available in [ASCII format](#).

Table T2. Results of geochemical analysis, Site 1085.

Leg, hole, core, section, interval (cm)	Depth (mbsf)	CaCO ₃ (%)	TOC (%)	MAR bulk sediment (g/[cm ² × k.y.])	MAR CaCO ₃ (g/[cm ² × k.y.])	MAR TOC (g/[cm ² × k.y.])	C/N (atomic)
175-1085A-28H-1, 52	251.22	63.40	1.33	10.618	6.73	141.33	
175-1085A-28H-1, 102	251.72	51.29	1.57	10.807	5.54	169.73	
175-1085A-28H-2, 2	252.22	62.82	1.23	10.997	6.91	134.91	
175-1085A-28H-2, 52	252.72	71.76	0.68	11.092	7.96	75.07	
175-1085A-28H-2, 102	253.22	70.09	0.93	11.186	7.84	104.55	
175-1085A-28H-3, 2	253.72	73.26	0.95	14.542	10.65	137.85	
175-1085A-28H-3, 52	254.22	67.25	1.04	14.664	9.86	152.79	
175-1085A-28H-3, 102	254.72	53.81	1.48	14.664	7.89	216.83	
175-1085A-28H-4, 2	255.22	56.60	1.33	14.664	8.30	195.60	
175-1085A-28H-4, 52	255.72	56.42	1.54	14.786	8.34	228.34	
175-1085A-28H-4, 102	256.22	68.55	1.07	14.908	10.22	159.95	
175-1085A-28H-5, 2	256.72	66.79	1.20	14.664	9.79	176.35	
175-1085A-28H-5, 52	257.22	59.45	1.53	14.664	8.72	224.56	
175-1085A-28H-5, 102	257.72	62.32	1.17	14.908	9.29	174.43	13.45
175-1085A-28H-6, 2	258.22	70.00	1.09	9.789	6.85	106.70	13.38
175-1085A-28H-6, 52	258.72	71.75	1.39	9.708	6.97	134.94	14.5
175-1085A-28H-6, 102	259.22	67.34	1.57	9.708	6.54	152.42	14.34
175-1085A-29H-1, 2	260.22	85.93	0.93	9.061	7.79	84.27	14.18
175-1085A-29H-1, 52	260.72	82.69	1.37	9.061	7.49	124.13	16
175-1085A-29H-1, 102	261.22	75.44	2.55	9.061	6.84	231.05	16.04
175-1085A-29H-2, 2	261.72	76.93	1.24	9.061	6.97	112.35	
175-1085A-29H-2, 52	262.22	77.90		8.232	6.41	0.00	
175-1085A-29H-2, 102	262.72	77.30	0.83	8.232	6.36	68.33	14.47
175-1085A-29H-3, 2	263.22	77.87	0.73	8.232	6.41	60.09	11.08
175-1085A-29H-3, 52	263.72	73.75	0.89	8.306	6.13	73.92	14.76
175-1085A-29H-3, 102	264.22	83.73	0.57	8.232	6.89	46.92	13
175-1085A-29H-4, 2	264.72	83.52	0.92	8.232	6.88	75.73	13.22
175-1085A-29H-4, 52	265.22	80.17	0.81	8.232	6.60	66.68	13.27
175-1085A-29H-4, 102	265.72	74.98	0.77	8.379	6.28	64.52	12.57
175-1085A-29H-5, 2	266.22	76.05	0.75	8.379	6.37	62.84	10.23
175-1085A-29H-5, 52	266.72	78.30	0.77	8.379	6.56	64.52	12.68
175-1085A-29H-5, 102	267.22	75.66	1.00	9.975	7.55	99.75	14.27
175-1085A-29H-6, 2	267.72	73.07	1.05	5.746	4.20	60.33	12.43
175-1085A-29H-6, 52	268.22	79.64	0.37	5.746	4.58	21.26	8.24
175-1085B-29H-6, 2	268.42	75.67	0.74	5.746	4.35	42.50	
175-1085B-29H-6, 102	268.72	78.12	0.96	5.746	4.49	55.16	12.48
175-1085B-29H-6, 52	268.92	75.23	0.91	5.746	4.32	52.27	
175-1085A-29H-7, 2	269.22	70.98	1.14	5.746	4.08	65.50	14.15
175-1085B-29H-6, 102	269.42	79.48	0.69	5.746	4.57	39.42	
175-1085B-29H-7, 2	269.92	85.22	0.63	5.746	4.90	36.33	
175-1085B-29H-7, 52	270.40	86.66	0.82	5.654	4.90	46.20	
175-1085B-30H-1, 2	270.42	82.77	0.37	5.654	4.68	20.70	
175-1085B-30H-1, 50	270.90	77.01	0.43	5.654	4.35	24.25	
175-1085B-30H-1, 100	271.40	71.55	0.63	5.654	4.05	35.79	
175-1085B-30H-2, 2	271.92	66.83	0.58	5.654	3.78	32.80	
175-1085B-30H-2, 52	272.42	72.10	0.74	5.654	4.08	42.04	
175-1085B-30H-2, 102	272.92	81.93	0.39	5.654	4.63	22.18	
175-1085B-30H-3, 2	273.42	87.32	0.43	5.654	4.94	24.41	
175-1085B-30H-3, 52	273.92	74.48	0.82	9.382	6.99	77.13	
175-1085B-30H-3, 102	274.42	75.68	0.54	9.382	7.10	50.38	
175-1085B-30H-4, 2	274.92	76.53	0.52	9.382	7.18	48.88	
175-1085B-30H-4, 52	275.42	75.82	0.66	9.382	7.11	61.76	
175-1085B-30H-4, 102	275.92	75.08	0.59	9.382	7.04	55.74	
175-1085B-30H-5, 2	276.42	80.36	0.50	9.382	7.54	47.35	
175-1085B-30H-5, 52	276.92	82.77	0.69	9.382	7.77	65.13	
175-1085B-30H-5, 102	277.42	81.77	0.93	7.695	6.29	71.21	
175-1085B-30H-6, 2	277.92	77.76	1.24	7.695	5.98	95.76	
175-1085B-30H-6, 52	278.42	75.89	0.85	7.695	5.84	65.72	
175-1085B-30H-6, 102	278.92	69.63	0.80	7.695	5.36	61.27	
175-1085A-31H-1, 2	279.22	91.94	0.31	7.695	7.07	23.85	13.2
175-1085B-30H-7, 2	279.42	72.36	0.74	7.695	5.57	56.58	
175-1085A-31H-1, 52	279.72			7.695	0.00	0.00	
175-1085A-31H-1, 102	280.22	74.76	0.82	7.695	5.75	63.10	12.95
175-1085A-31H-2, 2	280.72	76.71	0.76	7.965	6.11	60.53	10.91

Notes: CaCO₃ = calcium carbonate, TOC = total organic carbon, MAR = mass accumulation rate, C/N = carbon/nitrogen ratio. Only a portion of this table appears here. The entire table is available in [ASCII format](#).

Table T3. Results of organic carbon isotope analyses, Site 1085.

Core, section, interval (cm)	Depth (mbsf)	TOC (%)	C/N (atomic)	$\delta^{13}\text{C}_{\text{org}}$ (per mL)	Core, section, interval (cm)	Depth (mbsf)	TOC (%)	C/N (atomic)	$\delta^{13}\text{C}_{\text{org}}$ (per mL)
175-1085A-					35X-5, 142	321.22	0.70	9.85	-21.64
33H-3, 102	302.22	0.74	8.79	-21.54	35X-6, 92	322.22	0.72	10.02	-20.83
33H-4, 2	302.72	0.78	8.78	-22.11	35X-6, 142	322.72	1.00	11.83	-21.87
33H-4, 102	303.72	0.82	8.98	-21.88	35X-7, 42	323.22	0.57	9.97	-21.98
33H-5, 2	304.22	1.01	9.33	-21.65	35X-7, 92	323.72	0.60	10.47	-22.44
33H-5, 52	304.72	1.17	10.30	-22.11	35X-7, 142	324.22	0.62	10.38	-22.89
34X-1, 22	305.22	0.71	9.31	-21.01	36X-1, 32	324.72	0.66	9.35	-23.26
34X-1, 72	305.72	0.78	9.94	-21.78	36X-1, 84	325.22	0.60	7.53	-22.39
34X-1, 122	306.22	0.74	9.96	-21.18	36X-1, 132	325.72	0.56	7.52	-22.84
34X-2, 22	306.72	0.93	11.65	-21.86	36X-2, 32	326.22	0.84	9.68	-21.92
34X-2, 72	307.22	1.20	13.13	-21.11	36X-2, 82	326.72	1.12	11.67	-21.82
34X-2, 122	307.72	1.40	12.98	-21.04	36X-2, 132	327.22	0.65	9.15	-21.31
34X-3, 22	308.22	1.01	11.21	-21.74	36X-3, 32	327.72	0.70	8.60	-22.10
34X-3, 72	308.72	0.71	9.24	-22.29	36X-3, 132	328.72	0.57	8.12	-21.41
34X-3, 122	309.22	0.75	9.32	-22.03	36X-4, 32	329.22	0.79	10.07	-21.66
34X-4, 22	309.72	0.83	9.38	-21.54	36X-4, 82	329.72	0.92	11.87	-21.42
34X-4, 72	310.22	1.12	11.80	-21.47	36X-4, 132	330.22	1.01	12.11	-21.49
34X-4, 122	310.72	1.03	11.52	-21.73	36X-5, 32	330.72	1.19	12.08	-21.26
34X-5, 22	311.22	0.75	10.34	-22.39	36X-5, 82	331.22	0.88	10.15	-20.76
34X-5, 122	312.22	1.01	12.32	-21.48	36X-5, 132	331.72	0.93	10.03	-21.26
34X-6, 22	312.72	0.95	11.43	-22.91	36X-6, 32	332.22	0.97	9.55	-20.80
34X-6, 68	313.18	0.74	9.58	-22.21	36X-6, 82	332.72	0.67	8.53	-22.93
34X-6, 122	313.72	0.62	8.97	-22.03	36X-6, 132	333.22	0.53	8.18	-23.69
34X-7, 22	314.22	0.68	10.68	-21.74	37X-1, 20	334.20	0.75	10.08	-23.45
35X-1, 2	314.72	0.71	9.13	-22.24	37X-1, 73	334.73	0.51	7.66	-23.20
35X-1, 52	315.22				37X-1, 118	335.18	0.54	7.91	-22.99
35X-2, 42	315.72	0.84	10.68	-21.59	37X-2, 19	335.69	0.57	9.58	-23.12
35X-2, 92	316.22	0.76	9.54	-21.79	37X-2, 68	336.18	0.58	8.33	-20.14
35X-2, 142	316.72	0.72	10.23	-21.06	37X-2, 121	336.71	0.89	9.68	-21.26
35X-3, 92	317.72	0.83	10.30	-20.10	37X-3, 17	337.17	0.89	9.09	-21.33
35X-3, 142	318.22	0.67	10.30	-21.45	37X-3, 65	337.65	0.63	9.57	-22.89
35X-4, 42	318.72	0.80	9.45	-20.67	37X-3, 117	338.17	0.67	9.65	-22.97
35X-4, 92	319.22	0.69	9.32	-21.89	37X-4, 21	338.71	0.77	10.24	-21.95
35X-4, 142	319.72	1.05	11.28	-21.31	37X-4, 74	339.24	0.48	8.02	-24.13
35X-5, 42	320.22	0.54	8.01	-20.86	37X-4, 125	339.75	0.56	8.28	-22.24
35X-5, 92	320.72	0.50	8.07	-21.34					